THE JOURNAL OF PHYSICAL CHEMISTRY B

Article

pubs.acs.org/JPCB

Supramolecular and Redox Chemistry of Tetrathiafulvalene Monocarboxylic Acid with Hydrogen-Bonded Pyridine and Bipyridine Molecules

Qin-Yu Zhu,*[,†,‡] Qiong-Hua Han,[†] Ming-Yan Shao,[†] Jing Gu,[†] Zheng Shi,[†] and Jie Dai*[,†,‡]

[†]Department of Chemistry & Key Laboratory of Organic Synthesis of Jiangsu Province, Soochow University, Suzhou 215123, P. R. China

[‡]State Key Laboratory of Coordination Chemistry, Nanjing University, Nanjing 210093, P. R. China

Supporting Information

ABSTRACT: Although tetrathiafulvalene derivatives (TTFs) have been used as the redox-active unit in a lot of ion responsive receptors, only a few such examples of TTF carboxylic acids have been reported, especially about the responses to neutral organic molecules. In this work, electrochemical and spectral properties of dimethylthio-tetrathiafulvalene monocarboxylic acid (DMT-TTFCOOH) have been studied by both experimental methods and quantum chemical calculations. A square mechanism of proton transfer and electron transfer equilibriums was proposed. It is noteworthy that the process of oxidizing the TTF moiety of DMT-TTFCOOH could be controlled to obtain $TTF^{\bullet+}$ radical cation or TTF^{2+} dication by choosing suitable oxidizing reagents. Supramolecular responsive properties of DMT-TTFCOOH to py/bpy were investigated by cyclic voltammetry and ^1H NMR spectra. The results showed that the compound DMT-TTFCOOH is an electrochemically sensitive hydrogen bonding donor that can detect a tiny difference in the hydrogen bonding acceptor molecules. The theoretical calculations further confirm the results. The hydrogen-bonding structure of DMT-TTFCOOH-bpy in crystal was solved by X-ray diffraction analysis.

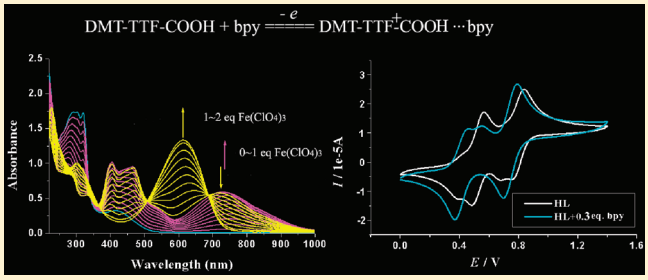

1. INTRODUCTION

Tetrathiafulvalene (TTF) and its derivatives (TTFs) are known to be strong π-donors capable of forming persistent radicals, thus making them a key component for molecular materials presenting various physical properties, such as photovoltaic,[1] magnetic, or NLO[2] properties, and leading to a broad range of applications.[3] Recently, the TTF system has aroused a renewed interest in various kinds of TTF-based ion sensors and switches, which are designed to associate an ion binding unit. The cyclic voltammogram (CV) of TTFs shows two pairs of reversible one-electron redox waves upon oxidation, corresponding to $TTF^{\bullet+}$/TTF and TTF^{2+}/$TTF^{\bullet+}$, accompanied with a spectral change, which could be tuned upon ionic guests binding. The pioneer and most research work in this context are that the crown-ether-TTF derivatives selectively bind some cations.[4] Several examples of pyridine-TTF derivatives have been designed, and their recognition behaviors for lead(II) have been studied.[5] Besides, pyrrolo-TTFs are also being explored and used for applications in cation and anion sensors.[6]

In comparison with the reported numerous researches of TTFs bearing different groups (thiolate,[7] phosphine,[7a,8] and pyridyl[7a,9]) for varied purposes, only a few studies on carboxylate-TTFs were carried out. Two complexes (M = Rh,[10a] Gd[10b]) based on monocarboxylate-TTFs, five complexes (M = Ni, Co,[11a] Mg, Ca,[11b] Na[11c]) based on dicarboxylate-TTFs, and some complexes (M = Zn,[12a] Cu, Mn,[12b] K, Ru, Cs,[12c] Co, Ni[12d]) based on tetracarboxylate-TTFs have been explored, but only two examples have been investigated as responsive ligands in solution. The group of Tian reported a supramolecular photoswitch containing monocarboxylate-TTFs.[13] We have reported a sodium(I) salt of dimethylthio-TTF dicarboxylate that is responsive to a benzotriazole molecule.[11c] Therefore, the related research of carboxylate-TTFs is largely undeveloped.

Our group has been engaged in the coordination compounds and responsive systems of TTFs, especially of carboxylate-TTFs.[11,12b] Herein, we describe a new supramolecular system constructed by an intermolecular hydrogen-bonding interaction between dimethylthio-TTF monocarboxylic acid (DMT-TTFCOOH) (DMT-TTFCOOH = $C_9H_8O_2S_6$) (Chart 1) and pyridine (py) or 4,4′-bipyridine (bpy). Pyridine groups have been widely used for supramolecular assembling with carboxylic acids via intermolecular hydrogen bonds.[14] Until now, however, very few redox-active responsive systems of carboxylate derivatives for *N*-heterocycle molecules have been reported.[11c,13] The redox active acid−base supramolecular interaction are important in biosystems, which prompt us to study the redox responsive behavior of TTF-carboxylic acid in the copresence of bpy/py molecules. The interest is also in that, although TTF has already

Received: December 23, 2011
Revised: March 15, 2012
Published: March 21, 2012

Chart 1. Structure of DMT-TTFCOOH

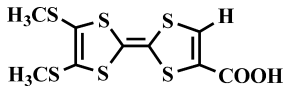

been used as the redox-active unit in a lot of ion responsive receptors,[4−6] to the best of our knowledge, few examples have been reported about TTFs responses to neutral organic molecules.[11c,13,15] Therefore, the electrochemical study of redox-active TTF responses for neutral organic molecules is a particular challenge. However, since Batail group reported the synthesis of DMT-TTFCOOH in 2004,[16] as an important TTF derivative, neither the chemical properties nor its electronic state has yet been studied in detail. In this article, we synthesized the compound DMT-TTFCOOH using the modified method reported by Batail group. The electrochemical and spectral properties of DMT-TTFCOOH have been studied by both experimental methods and quantum chemical calculations. The specific sensing properties of DMT-TTFCOOH for py and bpy were evaluated using different methods including cyclic voltammetry (CV) and ^{1}H NMR.

2. EXPERIMENTAL SECTION

2.1. General Remarks. The precursor, 2-(methyl-carboxylate)-6,7-bimethylthio-tetrathiafulvalene, DMT-TTF(CO_2Me), was prepared according to a reported method.[17] Standard deionized water was used for syntheses of the complexes. HPLC grade solvents (Alfa Aesar) were used for measurements of electrochemistry and spectra. All other reagents or solvents for syntheses and analyses were of analytical grade and used as received. The IR spectra were recorded as KBr pellets on a Nicolet Magna 550 FT-IR spectrometer. Elemental analyses of C, H, and N were performed using an EA1110 elemental analyzer. Electronic absorption spectra were measured on a Shimadzu UV-3150 spectrometer. ^{1}H NMR spectra were measured in $CDCl_3$−CD_3CN (1:1 by volume) using TMS as an internal standard on UNITYNOVA-400 spectrophotometer. Cyclic voltammetry (CV) experiments were performed on a CHI600 electrochemistry workstation in a three-electrode system, a Pt plate as the working electrode, a Pt wire as the auxiliary electrode, and a saturated calomel electrode (SCE) as the reference electrode. Density functional theory (DFT) calculations were carried out using the Gaussian03 program package.[18] All calculations were performed using B3LYP,[19] together with the 6-311G** basis set for DMT-TTFCOOH, DMT-TTF$^{\bullet+}$COOH, DMT-TTF^{2+}COOH, and 6-31G* basis set for DMT-TTFCOOH-py and DMT-TTFCOOH-bpy. The choice of this functional set is due to its satisfactory calculation of the energy of orbitals.

2.2. Synthesis of Compounds. *2.2.1. DMT-TTFCOOH.* A solution of DMT-TTF(CO_2Me) (0.0878 g, 0.248 mmol) in 1,4-dioxane (10 mL) was added a solution of LiOH (0.08 g, 3.3 mmol) in water (1 mL) under stirring. After stirring for 16 h at room temperature, the mixture was added 5 mol·L^{-1} HCl until the color turned from yellow to violet, and the solution was further stirred for 15 min. Then, water (20 mL) was added and a violet precipitate formed, collected by filtration, washed with water, and dried in vacuo to give product 0.07 g (yield: 86.3%). Anal. Calcd. for $C_9H_8O_2S_6$ (MW, 340.52): C, 31.75; H, 2.37. Found: C, 31.58; H, 2.17. IR data (cm^{-1}): 3080(w), 2970(w), 2917(w), 1665(s), 1553(m), 1527(m), 1429(m), 1300(s), 1194(m), 885(w), 834(w), 776(w), and 725(m).

2.2.2. DMT-TTFCOOH-bpy. A methanol (6 mL) solution of DMT-TTFCOOH (3.4 mg, 0.01 mmol) and bpy (3.1 mg, 0.02 mmol) was stirred for 0.5 h at room temperature and filtered. Red single crystals of DMT-TTFCOOH-bpy suitable for X-ray crystallography determination were obtained for 10 days from the filtrate by controlled evaporation of the solvent (3.4 mg, yield: 80.9%). Anal. Calcd. for $C_{28}H_{24}N_2O_4S_{12}$ (MW, 837.21): C, 40.17; H, 2.89; N, 3.35%. Found: C, 40.10; H, 2.91; N, 3.32%. IR data (cm^{-1}): 3064(w), 2914(m), 2854(w), 1695(s), 1599(m), 1564(m), 1535(m), 1520(w), 1482(w), 1460(w), 1434(m), 1320(m), 1191(m), 1056(m), 997(m), 874(m), 826(m), 834(w), 795(s), and 730(m).

2.3. X-ray Crystallographic Study. The measurement was carried out on a Rigaku Mercury CCD diffractometer at low temperature with graphite monochromated Mo Kα (λ = 0.71073 Å) radiation. X-ray crystallographic data for compound DMT-TTFCOOH-bpy were collected and processed using CrystalClear (Rigaku).[20] The structure was solved by direct methods using SHELXS-97,[21] and the refinement against all reflections of the compound was performed using SHELXL-97.[22] All the non-H atoms were refined in the anisotropic approximation against F^2 of all reflections. The H-atoms, except those attached to oxygen atoms, were placed at their calculated positions and refined in the isotropic approximation. The H-atoms attached to oxygen atoms were located in the difference Fourier maps and refined with isotropic displacement coefficients. Relevant crystal data, collection parameters, and refinement results can be found in Table 1. Selected bond lengths and bond angles are listed in Table 2 and Table 3, respectively.

Table 1. Crystal Data and Structural Refinement Parameters for DMT-TTFCOOH-bpy

formula	$C_{28}H_{24}N_2O_4S_{12}$	Z	4
fw	837.21	ρ_{calcd} (g cm^{-3})	1.568
cryst size (mm^3)	0.10 × 0.40 × 0.40	F(000)	1720
cryst syst	monoclinic	μ (mm^{-1})	0.777
space group	$P2/c$	T (K)	223(2)
a (Å)	22.440(2)	reflns collected	19 070
b (Å)	5.2005(4)	unique reflns	8056
c (Å)	31.963(3)	observed reflns	6210
α (deg)	90.00	no. params	428
β (deg)	107.996(2)	GOF on F^2	1.093
γ (deg)	90.00	R_1 [$I > 2\sigma(I)$]	0.0643
V (Å^3)	3547.5(6)	wR_2 [$I > 2\sigma(I)$]	0.1255

3. RESULTS AND DISCUSSION

3.1. Frontier Orbitals for DMT-TTFCOOH, DMT-TTF$^{\bullet+}$COOH, DMT-TTF^{2+}COOH, DMT-TTFCOOH-py, and DMT-TTFCOOH-bpy. In order to elucidate the electronic spectra and electrochemical properties, quantum chemical calculations were performed for DMT-TTFCOOH, DMT-TTF$^{\bullet+}$COOH, DMT-TTF^{2+}COOH, DMT-TTFCOOH-py, and DMT-TTFCOOH-bpy. The geometries were optimized by performing DFT calculations at the B3LYP/6-311G** level for DMT-TTFCOOH, DMT-TTF$^{\bullet+}$COOH, and DMT-TTF^{2+}COOH, and at the B3LYP/6-31G* level for DMT-TTFCOOH-py and DMT-TTFCOOH-bpy (SI-Figure 1, Supporting Information). DFT calculations include correlation effects at a relatively low computational cost and are known to provide accurate equilibrium geometries.[23] Comparing the experimental data with the calculated results for the main bond lengths and bond angles, only small differences were found. Therefore, on the basis of the geometries of the compounds obtained from the full optimization computations, the studies on

dx.doi.org/10.1021/jp2124179 | J. Phys. Chem. B 2012, 116, 4239−4247

Table 2. Selected Bond Lengths (Å) of DMT-TTFCOOH-bpy

S1−C1	1.748(4)	C3−C4	1.339(5)
S1−C3	1.765(4)	C5−C6	1.335(5)
S2−C2	1.724(4)	C9−O1	1.203(5)
S2−C3	1.755(4)	C9−O2	1.319(5)
S3−C4	1.753(4)	C10−C11	1.335(5)
S3−C5	1.756(4)	C10−C18	1.489(5)
S4−C6	1.758(4)	C12−C13	1.335(5)
S4−C4	1.759(4)	C14−C15	1.344(5)
S7−C10	1.742(4)	C18−O4	1.213(5)
S7−C12	1.755(4)	C18−O3	1.300(5)
S8−C11	1.729(4)	C10−C18	1.489(5)
S8−C12	1.762(4)	C12−C13	1.335(5)
S9−C13	1.752(4)	C14−C15	1.344(5)
S9−C14	1.756(4)	N1−C23	1.307(6)
S10−C15	1.748(4)	N1−C19	1.332(6)
S10−C13	1.763(4)	N2−C28	1.320(6)
C1−C2	1.328(6)	N2−C24	1.320(6)
C1−C9	1.486(6)		

Table 3. Selected Bond Angles (deg) of DMT-TTFCOOH-bpy

C1−S1−C3	94.22(18)	S5−C5−S3	117.5(2)
C2−S2−C3	94.88(19)	C5−C6−S4	117.4(3)
C4−S3−C5	95.77(18)	S4−C6−S6	117.4(2)
C6−S4−C4	95.52(18)	O1−C9−O2	125.5(4)
C10−S7−C12	94.49(18)	O1−C9−C1	122.0(4)
C11−S8−C12	94.51(18)	O2−C9−C1	112.5(4)
C13−S9−C14	95.20(17)	C11−C10−C18	125.4(4)
C15−S10−C13	95.13(17)	C11−C10−S7	117.7(3)
C23−N1−C19	117.1(4)	C18−C10−S7	116.9(3)
C28−N2−C24	116.8(4)	C10−C11−S8	118.3(3)
C2−C1−C9	125.4(4)	C13−C12−S7	121.1(3)
C2−C1−S1	117.7(3)	C13−C12−S8	123.9(3)
C9−C1−S1	116.9(3)	S7−C12−S8	114.9(2)
C1−C2−S2	118.5(3)	C12−C13−S9	123.2(3)
C4−C3−S2	122.2(3)	C12−C13−S10	122.2(3)
C4−C3−S1	123.2(3)	S9−C13−S10	114.6(2)
S2−C3−S1	114.6(2)	C15−C14−S9	117.4(3)
C3−C4−S3	122.6(3)	C14−C15−S10	117.5(3)
C3−C4−S4	123.3(3)	O4−C18−O3	125.9(4)
S3−C4−S4	114.1(2)	O4−C18−C10	122.5(4)
C6−C5−S3	117.2(3)	O3−C18−C10	111.6(3)

the molecular orbitals and related properties were carried out reasonably.

Figure 1 displays the atomic orbital composition calculated for the highest occupied molecular orbitals (HOMO − 1 and HOMO) and the lowest-unoccupied molecular orbitals (LUMO, LUMO + 1) of DMT-TTFCOOH, DMT-TTF$^{\bullet+}$COOH, and DMT-TTF^{2+}COOH, respectively. The frontier orbitals calculated for DMT-TTFCOOH-py and DMT-TTFCOOH-bpy are shown in SI-Figure 2 (Supporting Information). For DMT-TTFCOOH, the HOMO spreads over the whole molecule and results from the bonding interaction of the HOMO of the carboxylate moiety with the HOMO of the TTF fragment. The HOMO − 1 corresponds to the HOMO − 1 of carboxylate moiety bondingly and antibondingly interacting with the TTF fragment. The LUMO is essentially distributed over the carboxylate−dithiole ensemble. Most of the electron density of the LUMO is shifted to the carboxylate moiety in comparison with that of the HOMO. Hence, the photoinduced HOMO → LUMO excitation should have a charge-transfer nature from the TTF unit to the carboxylate moiety. For the cation radical DMT-TTF$^{\bullet+}$COOH, the change in electron density distribution from HOMO to LUMO is similar to that of the neutral DMT-TTFCOOH.

3.2. Electronic Characterization. The UV−vis absorption spectrum of compound DMT-TTFCOOH in CH_3CN is shown in Figure 2 (red line). The compound has a moderately intense broad absorption band in the range of 370 to 550 nm, at $\lambda_{max} \approx$ 380−440 nm (Table 4). On the basis of the theoretical calculations of the electronic excited states of DMT-TTFCOOH by using the time-dependent DFT (TDDFT) approach, the HOMO → LUMO excitation gives rise to the lowest energy gap 2.68 eV (463 nm, f = 0.04), consistent with the observed band. According to the related orbital characters, the HOMO → LUMO one-electron promotion implies an electron density transfer from the dithiole ring (an electron donor) to the carboxylate moiety (an electron acceptor) and gives rise to an intramolecular charge-transfer band. The HOMO → LUMO + 2 excitation was calculated at 3.36 eV (368 nm, f = 0.02), which also contributes to the broad shape of the absorption band in 370 to 550 nm observed experimentally. Besides, the compound shows strong absorption bands at 300 and 317 nm, which belong to the local transition of TTF moiety. These bands originate in the HOMO − 1 → LUMO and HOMO − 1 → LUMO + 1 excitations. The excitations give rise to two electronic transitions calculated at 4.13 eV (300 nm, f = 0.04) and 3.97 eV (312 nm, f = 0.06), in good agreement with the observed bands.

3.3. Chemical Oxidation of DMT-TTFCOOH. Chemical oxidation of DMT-TTFCOOH in acetonitrile was carried out by successive addition of $Fe(ClO_4)_3 \cdot 6H_2O$ as oxidizing reagent[4b] (CAUTION: All metal perchlorates must be regarded as potentially explosive. Only a small amount of compound should be prepared, and it should be handled with caution). The changes of UV−vis spectra of the reaction system were recorded in Figure 2a. At first, the addition of increasing amounts of $Fe(ClO_4)_3 \cdot 6H_2O$ led to the development of a new band at 729 nm, which showed the characteristic band of the radical TTF$^{\bullet+}$ cation.[24] Calculations predict that one-electron transition from HOMO to LUMO of DMT-TTF$^{\bullet+}$COOH is at 1.63 eV (763 nm, f = 0.13). The energy levels of the entire set of MOs of DMT-TTF$^{\bullet+}$COOH dropped greatly due to the oxidation (SI-Table 1, Supporting Information), and a simultaneous reduction in energy gap ΔE ($E_{LUMO} - E_{HOMO}$) happened. Thus, the lower-energy gap results in the red shift of the absorption peak. The appearance of the isosbestic point at 343 nm reveals that there is a two-species equilibrium in this system: DMT-TTFCOOH and DMT-TTF$^{\bullet+}$COOH. When the addition of 1 equiv of Fe^{3+}, the intensity of the new band at 729 nm reaches the maximum.

Upon further addition of more than 1 equiv of Fe^{3+}, the absorption intensity at 729 nm started to decrease, and a new absorption band emerged at 613 nm. The absorption band around 613 nm is attributed to TTF^{2+}. The energy gap ΔE between HOMO and LUMO ($E_{LUMO} - E_{HOMO}$) of DMT-TTF^{2+}COOH is 1.89 eV (655 nm, f = 0.34). Meanwhile, neat isosbestic points at 365, 507, and 687 nm are observed, which indicates a new equilibrium between two absorbing species in the solution: DMT-TTF$^{\bullet+}$COOH and DMT-TTF^{2+}COOH.

Chemical oxidation in the same solvent was also carried out by the successive addition of $Cu(ClO_4)_2$ as the oxidizing reagent. In this case, the same characteristic band of the cation

dx.doi.org/10.1021/jp2124179 | J. Phys. Chem. B 2012, 116, 4239−4247

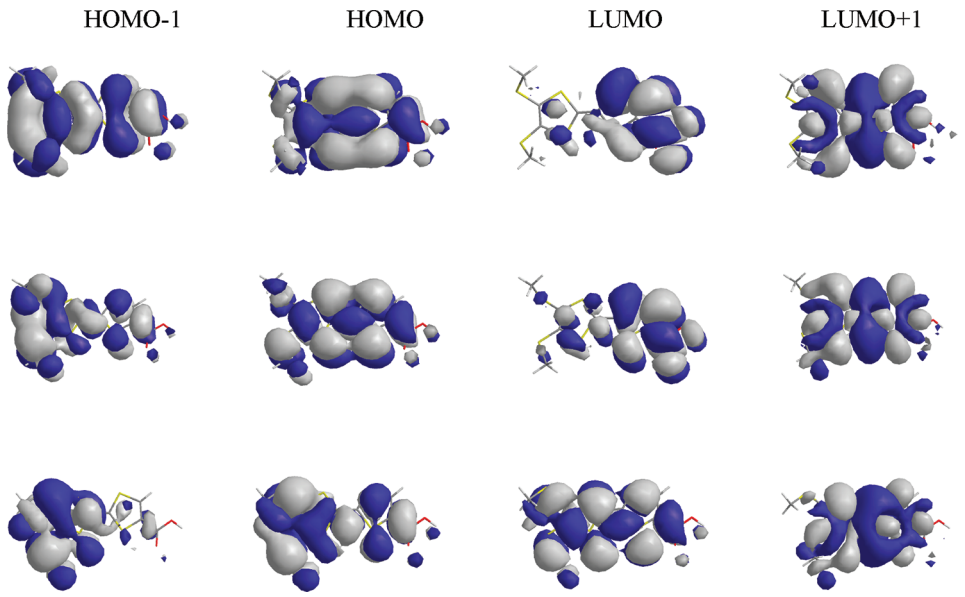

Figure 1. Frontier orbitals calculated for DMT-TTFCOOH (top), DMT-TTF$^{\bullet+}$COOH (middle), DMT-TTF^{2+}COOH (bottom).

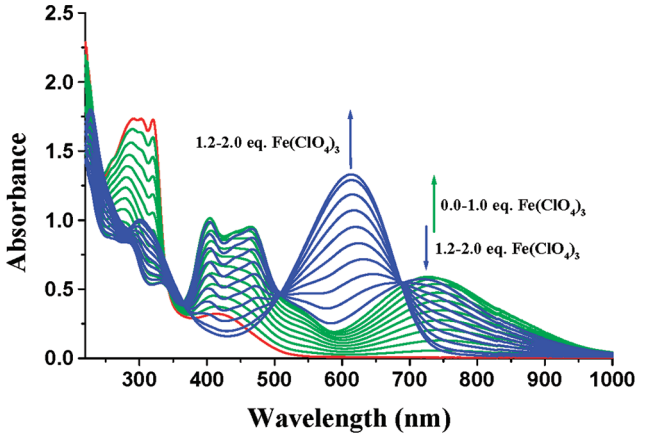

Figure 2. Changes of the UV−vis absorption of DMT-TTFCOOH (1.0×10^{-4} mol·L^{-1}) in CH_3CN, upon the addition of increasing amounts of (a) $Fe(ClO_4)_3 \cdot 6H_2O$ (from 0 to 2.0×10^{-4} mol·L^{-1}) and (b) $CuCl_2$ (from 0 to 3.0×10^{-4} mol·L^{-1}).

radical DMT-TTF$^{\bullet+}$ (731 nm) and dication DMT-TTF^{2+} (615 nm) are observed (SI-Figure 3, Supporting Information).

Table 4. Theoretical and Experimental UV−Vis Results (nm) of DMT-TTFCOOH, DMT-TTF$^{\bullet+}$COOH, and DMT-TTF^{2+}COOH (Data in Parentheses Represent the Oscillator Strength)

cmpd	theor	exptl
DMT-TTFCOOH	300(0.041), 312(0.064), 368(0.020), 463(0.038)	300, 317, 380−440
DMT-TTF$^{\bullet+}$COOH	440(0.016), 465(0.013), 692(0.004), 763(0.127)	401, 464, 729
DMT-TTF^{2+}COOH	362(0.057), 384(0.011), 527(0.062), 655(0.342)	302, 613

However, when the oxidizing reagent is replaced with $CuCl_2$ in the same solvent, only a new band at 740 nm can be observed. Upon the addition of 3 equiv of $CuCl_2$, the intensity of the new band reaches the limit, and no new band appears (Figure 2b). The result means that DMT-TTFCOOH can only be oxidized to the radical cation TTF$^{\bullet+}$ by $CuCl_2$ and cannot be further oxidized to dication TTF^{2+}. The reason might be that the Cu−Cl is covalently bonded so that the $CuCl_2$ could not be completely ionized as $Cu(ClO_4)_2$ in acetonitrile. The oxidizing ability of $CuCl_2$ is largely decreased in comparison with the free Cu^{2+} of $Cu(ClO_4)_2$. The results of the UV−vis of chemical oxidation of DMT-TTFCOOH indicate that the redox states of TTF derivatives could be controlled by choosing oxidizing reagents.

3.4. Redox Responses to py/bpy. The study of the electrochemical responses of TTFs to neutral molecules is largely undeveloped in comparison with those to ions. We conducted cyclic voltammetry (CV) studies to explore the responsive properties of DMT-TTFCOOH to py/bpy in CH_2Cl_2−CH_3CN (1:1 by volume) solution. The cyclic voltammogram (CV) of DMT-TTFCOOH showed two pairs of reversible one-electron redox waves typical of the TTF system, $E^1_{1/2}$ = 0.523 V and $E^2_{1/2}$ = 0.797 V (Figure 3, black line), corresponding to DMT-TTF$^{\bullet+}$COOH/DMT-TTFCOOH and DMT-TTF^{2+}COOH/DMT-TTF$^{\bullet+}$COOH that has been well-characterized of the redox properties of TTF derivatives. Unusually, the splitting of both reduction waves was recorded (Table 5), which was attributed to the occurrence of proton dissociation of carboxylic acid when the TTF unit undergoes the two-electron oxidation.

dx.doi.org/10.1021/jp2124179 | J. Phys. Chem. B 2012, 116, 4239−4247

Table 5. Oxidation and Reduction Peak Potentials of DMT-TTFCOOH (1.0×10^{-3} mol·L^{-1}) (0.1 mol·L^{-1} Bu_4NClO_4, 100 mV s^{-1}) in the Presence of 0.3 equiv of py/bpy in CH_2Cl_2/CH_3CN (1:1 by Volume)

cmpd	E^1_{ox}	$E^1_{ox}{}'$	E^2_{ox}	E^1_{red}	$E^1_{red}{}'$	E^2_{red}	$E^2_{red}{}'$
DMT-TTFCOOH	0.564		0.837	0.482	0.382	0.756	0.671
DMT-TTFCOOH + py	0.453		0.734	0.360		0.648	
DMT-TTFCOOH + bpy	0.453	0.556	0.796	0.364		0.697	

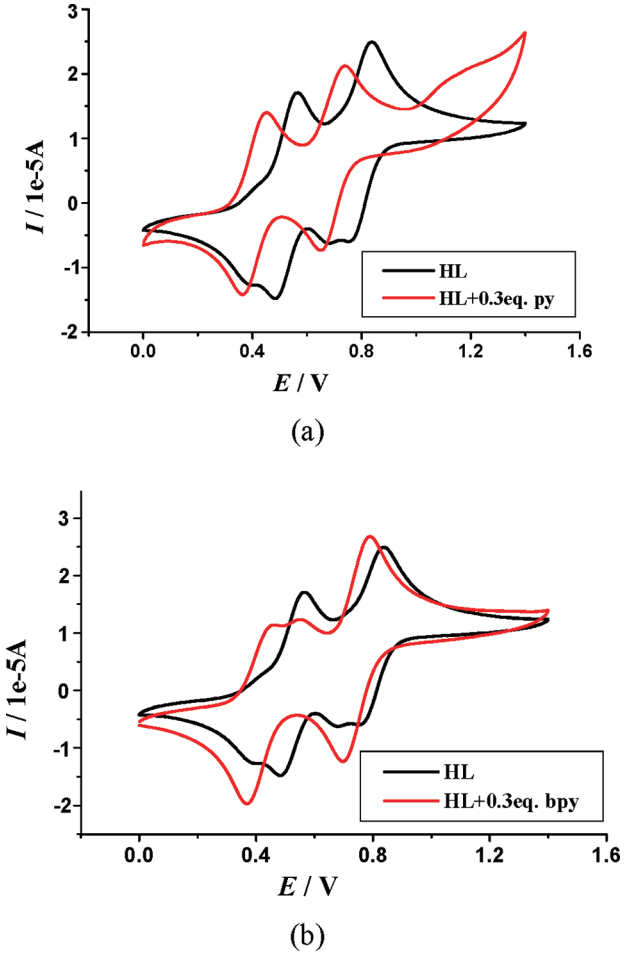

Figure 3. Cyclic voltammogram of DMT-TTFCOOH (HL) (1.0×10^{-3} mol·L^{-1}) (0.1 mol·L^{-1} Bu_4NClO_4, 100 mV s^{-1}) at a scan rate of 100 mV s^{-1} in the presence of 0.3 equiv (a) py and (b) bpy in CH_2Cl_2/CH_3CN (1:1 by volume).

There should be two other redox species: DMT-TTF$^{\bullet+}$COO$^-$ and DMT-TTF^{2+}COO$^-$. As soon as the two-electron reduction processes end, the proton goes back to the carboxylate group due to the decrease of the electrostatic repulsive interaction. The equilibrium processes of the proton transfer and the electron transfer are shown in the box in Scheme 1.

The addition of 0.3 equiv of py/bpy to the solution of DMT-TTFCOOH caused remarkable cathodic shifts in the CVs (Figure 3). In the case of py, substantial negative potential shifts of the two redox peaks were observed with $\Delta E_{1/2}(1)$ = 0.117 V for the first redox potential and with $\Delta E_{1/2}(2)$ = 0.106 V for the second redox potential (Figure 3a). It is noteworthy that the second oxidation peak is also negatively shifted, which is different from those of the responses of TTF derivatives to metal ions in which the E^1_{ox} value is usually shifted to higher potential and the E^2_{ox} value shows no obvious change whatever the amount of added metal because of the leaving of the guest

Scheme 1. Equilibrium Reaction during the Electrochemical Redox

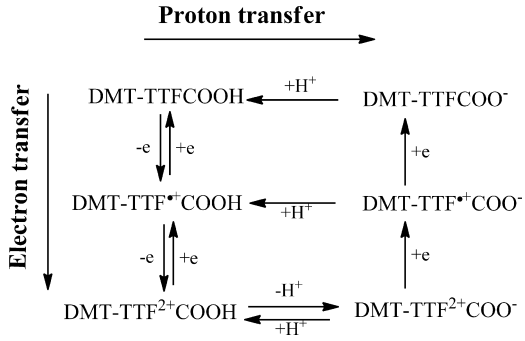

cation due to the increased electrostatic repulsion of TTF^{2+} cation.[25] The large negative potential shifts correspond to an increase in the π-donating ability of the TTF unit and indicate that the redox-active TTF moiety appears much easier to be oxidized upon adding py. The reason why the oxidation waves are shifted to more cathodic potentials is interpreted as being the result of the strong hydrogen bonding interaction between DMT-TTFCOOH (hydrogen bonding donor) and py (hydrogen bonding acceptor) that increases the electron density of the TTF moiety. Theoretical calculations also show that the HOMO energy of DMT-TTFCOOH-py (−4.79 eV) is higher than that of DMT-TTFCOOH (−5.20 eV). The higher the HOMO energy of DMT-TTFCOOH-py, the lower its E_{ox}. This result accounts for the more negative oxidation potentials measured for DMT-TTFCOOH-py in comparison with DMT-TTFCOOH.

As far as bpy is concerned, two redox potentials also cathodically shifted (Figure 3b). However, it was interestingly found that upon the addition of 0.3 equiv of bpy to the solution of DMT-TTFCOOH, a new oxidation peak of the TTF unit emerged at lower potential, while the first original oxidation peak current of the waves did not disappear as the case of py but only decreased. This is evidence that only part of DMT-TTFCOOH form hydrogen bonds with bpy. The different responses of DMT-TTFCOOH to py/bpy should be attributed to the small differences in basicity between py and bpy. From the distances (Figure 4) of N···H···O of the optimized geometry

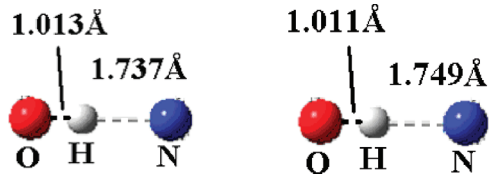

Figure 4. Distances of N···H and O···H of DMT-TTFCOOH-py (left) and DMT-TTFCOOH-bpy (right).

(Figure 5) of compounds DMT-TTFCOOH-py and DMT-TTFCOOH-bpy, we could see the same tiny differences. The distance of N···H of DMT-TTFCOOH-py is appreciably shorter

dx.doi.org/10.1021/jp2124179 | J. Phys. Chem. B 2012, 116, 4239–4247

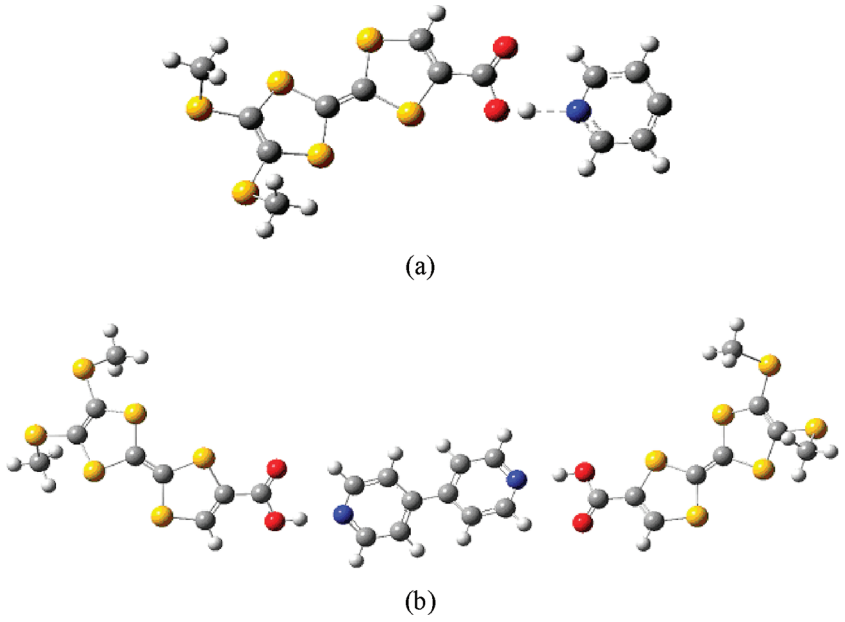

Figure 5. Minimum-energy conformations calculated at B3LYP/6-31G* level for DMT-TTFCOOH-py (a) and DMT-TTFCOOH-bpy (b).

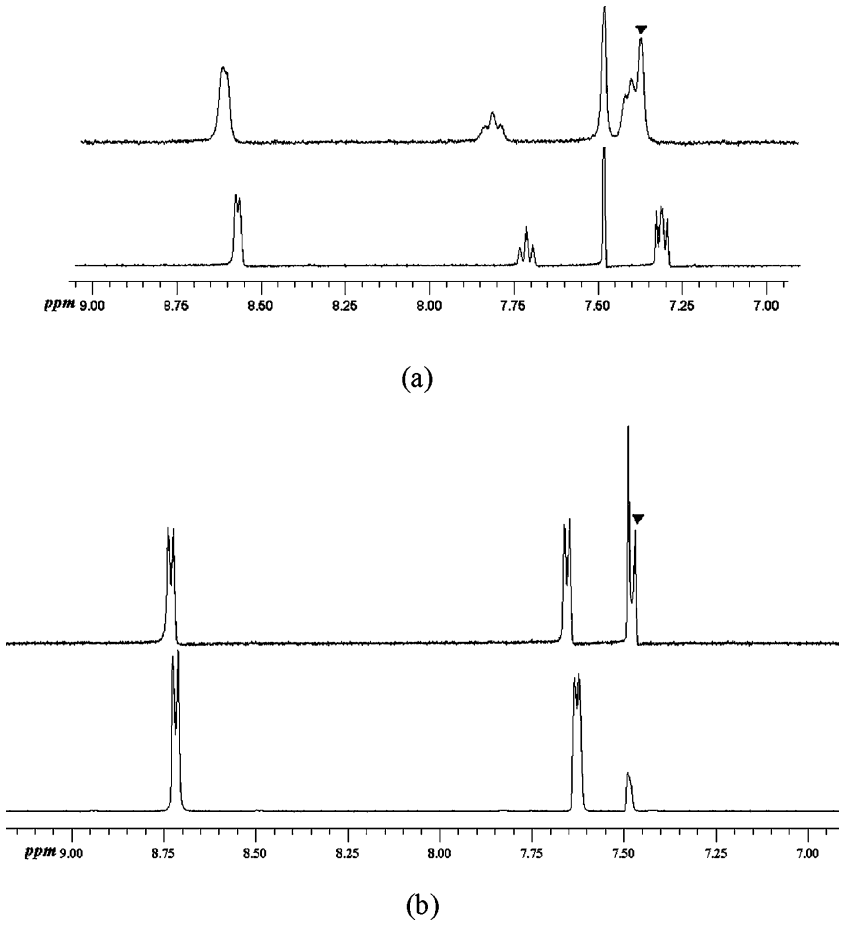

Figure 6. (a) ^{1}H NMR spectra in $CDCl_3$–CD_3CN (1:1 by volume) of (bottom) py, (top) DMT-TTFCOOH + 0.3 equiv of py; (b) (bottom) bpy, (top) DMT-TTFCOOH + 0.3 equiv of bpy.

than that of DMT-TTFCOOH-bpy, while the situation of the distance of O···H is in contrast. The theoretical calculation results further confirm that the ability of hydrogen bonding acceptor of py is slightly stronger than that of bpy. The different CV responses to py and bpy of DMT-TTFCOOH might be employed to construct a molecular sensor to response different *N*-heterocycle molecules, if using a carefully selected solvent system.

3.5. ^{1}H NMR Responses to py/bpy. To further confirm the selective sensing properties of DMT-TTFCOOH toward py and bpy, ^{1}H NMR experiments of DMT-TTFCOOH, py,

dx.doi.org/10.1021/jp2124179 | *J. Phys. Chem. B* 2012, 116, 4239–4247

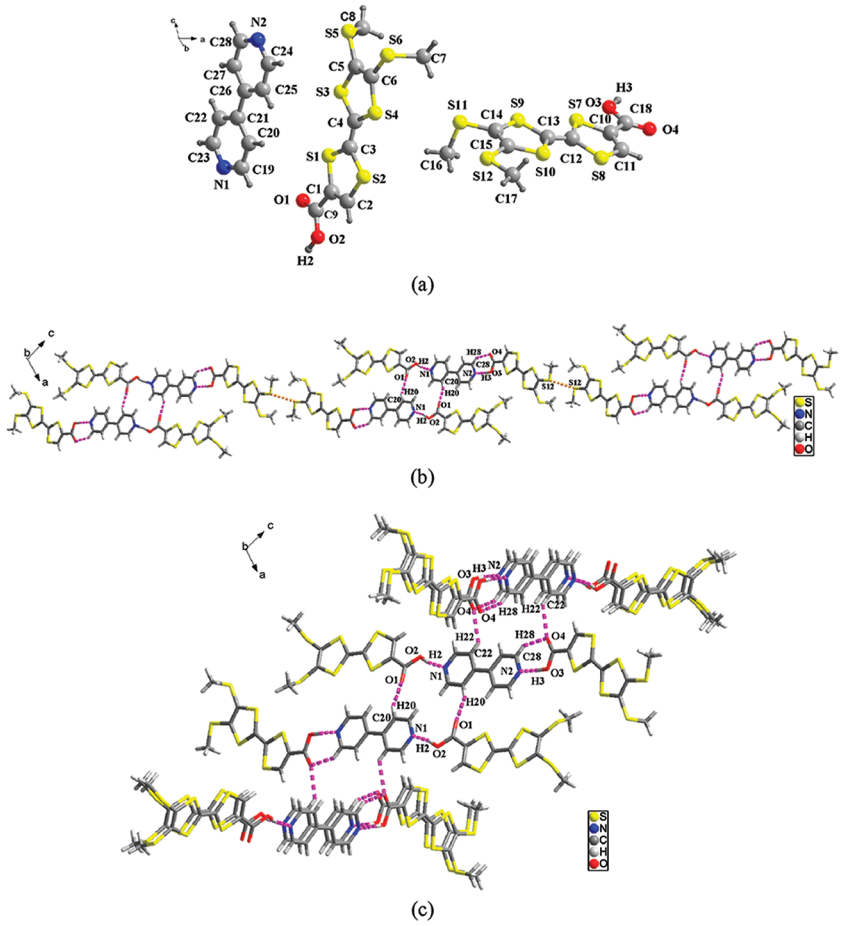

Figure 7. (a) Crystal structure of (4,4′-bpy)·2(DMT-TTFCOOH) with labeling scheme; (b) 1-D chain structure through O1···H20−C20 hydrogen bonds between dimers constructed by S12···S12 short contacts, showing the two different types of hydrogen bonding motifs for the carboxylate groups of DMT-TTFCOOH; (c) 2-D supramolecular structure through O4···H22−C22 hydrogen bonds between chains lied in the different orientation.

bpy, and DMT-TTFCOOH upon the addition of 0.3 equiv of py and bpy in $CDCl_3$−CD_3CN (1:1 by volume) were performed. Figure 6 shows a comparison of the partial ^1H NMR spectrum of (a) DMT-TTFCOOH upon the addition of 0.3 equiv of py with py and (b) DMT-TTFCOOH upon the addition of 0.3 equiv of bpy with bpy. The chemical shift of the resonance of C═C−H of the TTF unit located at 7.493 ppm was close to that of $CDCl_3$ (7.487 ppm). Upon the addition of 0.3 equiv of py, the C═C−H (denoted as ▼, overlapped with the partial spectrum of the *meta*-H of py) of the TTF unit shifted upfield distinctly ($\Delta\delta$ = 0.114 ppm); the H of pyridine also showed a distinct downfield shift ($\Delta\delta$ = 0.041, 0.099, and 0.102 ppm) (Figure 6a). While in the case of bpy, the C═C−H (denoted as ▼) of the TTF unit is also shifted upfield ($\Delta\delta$ = 0.026 ppm), and the H of bipyridine presented a downfield shift ($\Delta\delta$ = 0.016 and 0.029), but the changes are smaller as compared with those in the case of py (Figure 6b). These observations indicated that the interaction of the DMT-TTFCOOH with py is stronger than that with bpy. It is important to note that the difference of the response of the ^1H NMR spectra of DMT-TTFCOOH for py and bpy is specific.

3.6. Description of the Crystal Structure of DMT-TTFCOOH-bpy. The strength of hydrogen bonds is responsible for the different responsive behavior of DMT-TTFCOOH toward py/bpy. We have investigated the crystal structure of DMT-TTFCOOH-bpy, while the crystal of the compound DMT-TTFCOOH-py is poor and not suitable for X-ray measurement.

The compound DMT-TTFCOOH-bpy crystallizes in the monoclinic system, space group *P*2/*c*, with four chemical formulas in a unit cell. The molecular structure of DMT-TTFCOOH-bpy is depicted in Figure 7a. The compound comprises one bpy molecule and two independent DMT-TTFCOOH molecules located in the different orientations. From the Fourier map and the different C−O bond lengths, it can be concluded that the proton of the carboxylic acid has not been transferred to the pyridine group so that the H-bonding interaction can be described as involving a pyridine H-bond acceptor and a carboxylate H-bond donor. As shown in Figure 7b, each molecule of bpy bridges two adjacent molecules of DMT-TTFCOOH through O2−H2···N1, O3−H3···N2, and C28−H28···O4[26] (Table 6) hydrogen bonds to constitute a unit, showing the two different types of hydrogen bonding motifs for the carboxylate groups of DMT-TTFCOOH. A dimer is constructed by such two units through S12···S12 short contacts, and a one-dimensional chain is formed through O1···H20−C20 hydrogen bonds between dimers. The neighboring chains lying in the different orientation are connected together by O4···H22−C22 hydrogen bonds forming a 2-D supramolecular structure.

dx.doi.org/10.1021/jp2124179 | *J. Phys. Chem. B* 2012, 116, 4239−4247

Table 6. Distances (Å) and Angles (deg) of Hydrogen Bonds of (4,4′-bpy)·2(DMT-TTFCOOH)

	D−H	H···A	D···A	D−H···A
O2−H2···N1[a]	0.97	1.72	2.57	144
O3−H3···N2[b]	0.92	1.66	2.58	176
C20−H20···O1[c]	0.94	2.55	3.41	153
C22−H22···O4[d]	0.94	2.47	3.19	134
C28−H28···O4[e]	0.94	2.51	3.21	131

[a]Symmetry transformation used to generate equivalent atoms: x, $2 - y$, $1/2 + z$. [b]x, $-1 + y$, z. [c]$1 - x$, $2 + y$, $1/2 - z$. [d]$1 - x$, $-2 + y$, $1/2 - z$. [e]$1 - x$, $-1 + y$, $1/2 - z$.

4. CONCLUSIONS

In conclusion, the quantum chemical calculations, electronic spectra, electrochemical behavior, ^{1}H NMR spectra, and single crystal structure of a tetrathiafulvalene derivative, dimethylthio-tetrathiafulvalene monocarboxylic acid (DMT-TTFCOOH), were investigated. All the results show that (1) compound DMT-TTFCOOH can be oxidized to the radical cation $TTF^{\bullet+}$ or to the TTF^{2+} dication by choosing suitable oxidizing reagents, which could be used to control the process of oxidizing to obtain neutral TTF, $TTF^{\bullet+}$ radical cation, or TTF^{2+} dication; (2) it can undergo two-step electrochemical redox with a square mechanism of proton transfer and electron transfer equilibriums; and (3) the addition of py/bpy to the solution of DMT-TTFCOOH results in the different changes of the chemical shifts in ^{1}H NMR and the redox potentials in CV. It is an electrochemically sensitive hydrogen bonding donor that can detect tiny difference of the hydrogen bonding property of an acceptor molecule. Theoretical calculation results are consistent with the redox-responsive properties of DMT-TTFCOOH. The sensitive redox responses of DMT-TTFCOOH to *N*-heterocycle molecules make this compound a good candidate for constructing a molecular sensor to *N*-heterocycle hydrogen bonding acceptor molecules.

■ ASSOCIATED CONTENT

Supporting Information

Calculated structures, front and side views are presented; frontier orbitals calculated for DMT-TTFCOOH-py and DMT-TTFCOOH-bpy; changes of the UV−vis absorption of compound DMT-TTFCOOH (1.0×10^{-4} mol·L^{-1}) in CH_3CN, upon the addition of increasing amounts of $Cu(ClO_4)_2$ (from 0 to 3.2×10^{-4} mol·L^{-1}); changes of the UV−vis absorption of DMT-TTFCOOH (HL) (1.0×10^{-4} mol·L^{-1}) in CH_3CN, upon the addition of increasing amounts of py and bpy; theoretical energy levels and values including HOMO−LUMOs. This material is available free of charge via the Internet at http://pubs.acs.org.

■ AUTHOR INFORMATION

Corresponding Author

*E-mail: zhuqinyu@suda.edu.cn (Q.-Y.Z.); daijie@suda.edu.cn (J.D.).

Notes

The authors declare no competing financial interest.

■ ACKNOWLEDGMENTS

This work is supported by the NNS Foundation (21171127), the Priority Academic Program Development of Jiangsu Higher Education Institutions, and the Program of Innovative Research Team of Soochow University.

■ REFERENCES

(1) Martín, N.; Sánchez, L.; Herranz, M. A.; Illescas, B.; Guldi, D. M. *Acc. Chem. Res.* **2007**, *40*, 1015−1024.

(2) Garín, J.; Orduna, J.; Andreu, R. *Recent Res. Dev. Org. Chem.* **2001**, *5*, 77−87.

(3) (a) Yamada, J.-I.; Sugimoto, T., Eds. *TTF Chemistry: Fundamentals and Applications of Tetrathiafulvalene*; Springer: Berlin, Germany, 2004. (b) Nielsen, M. B.; Lomholt, C.; Becher, J. *Chem. Soc. Rev.* **2000**, *29*, 153−164. (c) Martín, N.; Segura, J.-L. *Angew. Chem., Int. Ed.* **2001**, *40*, 1372−1409. (d) Khodorkovsky, V.; Becker, J. Y. In *Organic Conductors: Fundamentals and Applications*; Farges, J. P., Ed.; Marcel Dekker: New York, 1994; Chapter 3. (e) William, J. M.; Ferraro, J. R.; Thorn, R. J.; Carlson, K. D.; Geiser, U.; Wang, H. H.; Kini, A. M.; Whangbo, M. H. *Organic Superconductors (Including Fullerenes): Synthesis Structure, Properties, and Theory*; Prentice Hall: Englewoods Cliffs, NJ, 1992.

(4) (a) Hansen, T. K.; Jørgensen, T.; Stein, P. C.; Becher, J. *J. Org. Chem.* **1992**, *57*, 6403−6409. (b) Jørgensen, T.; Hansen, T. K.; Becher, J. *Chem. Soc. Rev.* **1994**, *23*, 41−51. (c) Liu, S. G.; Echegoyen, L. *Eur. J. Org. Chem.* **2000**, 1157−1163. (d) Le Derf, F.; Mazari, M.; Mercier, N.; Levillain, E.; Richomme, P.; Becher, J.; Garín, J.; Orduna, J.; Gorgues, A.; Sallé, M. *Inorg. Chem.* **1999**, *38*, 6096−6100. (e) Lyskawa, J.; Le Derf, F.; Levillain, E.; Mazari, M.; Sallé, M.; Dubois, L.; Viel, P.; Bureau, C.; Palacin, S. *J. Am. Chem. Soc.* **2004**, *126*, 12194−12195. (f) Lyskawa, J.; Le Derf, F.; Levillain, E.; Mazari, M.; Sallé, M. *Eur. J. Org. Chem.* **2006**, 2322−2328.

(5) (a) Xue, H.; Tang, X.-J.; Wu, L.-Z.; Zhang, L.-P.; Tung, C.-H. *J. Org. Chem.* **2005**, *70*, 9727−9734. (b) Zhao, Y. P.; Wu, L. Z.; Si, G.; Liu, Y.; Xue, H.; Zhang, L. P.; Tung, C. H. *J. Org. Chem.* **2007**, *72*, 3632−3639. (c) Balandier, J.-Y.; Belyasmine, A.; Sallé, M. *Eur. J. Org. Chem.* **2008**, 269−276.

(6) (a) Nielsen, K. A.; Jeppesen, J. O.; Levillain, E.; Becher, J. *Angew. Chem., Int. Ed.* **2003**, *42*, 187−191. (b) Jeppesen, J. O.; Becher, J. *Eur. J. Org. Chem.* **2003**, 3245−3266. (c) Becher, J.; Jeppesen, J. O.; Nielsen, K. *Synth. Met.* **2003**, *133−134*, 309−313. (d) Trippé, G.; Levillain, E.; Derf, F. L.; Gorgues, A.; Sallé, M.; Jeppesen, J. O.; Nielsen, K.; Becher, J. *Org. Lett.* **2002**, *4*, 2461−2464. (e) Nielsen, K. A.; Cho, W.-S.; Jeppesen, J. O.; Lynch, V. M.; Becher, J.; Sessler, J. L. *J. Am. Chem. Soc.* **2004**, *126*, 16296−16297. (f) Nielsen, K. A.; Cho, W.-S.; Lyskawa, J.; Levillain, E.; Lynch, V. M.; Sessler, J. L.; Jeppesen, J. O. *J. Am. Chem. Soc.* **2006**, *128*, 2444−2451.

(7) (a) Lorcy, D.; Bellec, N.; Fourmigué, M.; Avarvari, N. *Coord. Chem. Rev.* **2009**, *253*, 1398−1438 and references therein. (b) Tanaka, H.; Okano, Y.; Kobayashi, H.; Suzuki, W.; Kobayashi, A. *Science* **2001**, *291*, 285−287. (c) Tanaka, H.; Kobayashi, H.; Kobayashi, A. *J. Am. Chem. Soc.* **2002**, *124*, 10002−10003. (d) McCullough, R. D.; Belot, J. A.; Rheingold, A. L.; Yap, G. P. A. *J. Am. Chem. Soc.* **1995**, *117*, 9913−9914.

(8) (a) Devic, T.; Batail, P.; Fourmigué, M.; Avarvari, N. *Inorg. Chem.* **2004**, *43*, 3136−3141. (b) Uzelmeier, C. E.; Smucker, B. W.; Reinheimer, E. W.; Shatruk, M.; O'Neal, A. W.; Fourmigué, M.; Dunbar, K. R. *Dalton Trans.* **2006**, 5259−5268. (c) Avarvari, N.; Martin, D.; Fourmigué, M. *J. Organomet. Chem.* **2002**, *643−644*, 292−300.

(9) (a) Iwahori, F.; Golhen, S.; Ouahab, L.; Carlier, R.; Sutter, J.-P. *Inorg. Chem.* **2001**, *40*, 6541−6542. (b) Setifi, F.; Ouahab, L.; Golhen, S.; Yoshida, Y.; Saito, G. *Inorg. Chem.* **2003**, *42*, 1791−1793. (c) Hervé, K.; Le Gal, Y.; Ouahab, L.; Golhen, S.; Cador, O. *Synth. Met.* **2005**, *153*, 461−464. (d) Jia, C.; Liu, S. X.; Ambrus, C.; Neels, A.; Labat, G.; Decurtins, S. *Inorg. Chem.* **2006**, *45*, 3152−3154. (e) Liu, S. X.; Ambrus, C.; Dolder, S.; Neels, A.; Decurtins, S. *Inorg. Chem.* **2006**, *45*, 9622−9624. (f) Gavrilenko, K. S.; Le Gal, Y.; Cador, O.; Golhen, S.; Ouahab, L. *Chem. Commun.* **2007**, 280−282. (g) Zhu, Q. Y.; Liu, Y.; Lu, W.; Zhang, Y.; Bian, G. Q.; Niu, G. Y.; Dai, J. *Inorg. Chem.* **2007**, *46*, 10065−10070.

(10) (a) Ebihara, M.; Nomura, M.; Sakai, S.; Kawamura, T. *Inorg. Chim. Acta* **2007**, *360*, 2345−2352. (b) Pointillart, F.; Le Gal, Y.; Golhen, S.; Cador, O.; Ouahab, L. *Chem. Commun.* **2009**, 3777−3779.

(11) (a) Gu, J.; Zhu, Q.-Y.; Zhang, Y.; Lu, W.; Niu, G.-Y.; Dai, J. *Inorg. Chem. Commun.* **2008**, *11*, 175−178. (b) Wang, J.-P.; Lu, Z.-J.; Zhu, Q.-Y.; Zhang, Y.-P.; Qin, Y.-R.; Bian, G.-Q.; Dai, J. *Cryst. Growth Des.* **2010**, *10*, 2090−2095. (c) Zhu, Q.-Y.; Lin, H.-H.; Dai, J.; Bian, G.-Q.; Zhang, Y.; Lu, W. *New J. Chem.* **2006**, *30*, 1140−1144.
(12) (a) Han, Y.-F.; Li, X.-Y.; Li, J.-K.; Zheng, Z.-B.; Wu, R. T.; Lu, J.-R. *Chin. J. Inorg. Chem.* **2009**, *25*, 1290−1294. (b) Qin, Y.-R.; Zhu, Q.-Y.; Huo, L.-B.; Shi, Z.; Bian, G.-Q.; Dai, J. *Inorg. Chem.* **2010**, *49*, 7372−7381. (c) Nguyen, T. L. A.; Demir-Cakan, R.; Devic, T.; Morcrette, M.; Ahnfeldt, T.; Auban-Senzier, P.; Stock, N.; Goncalves, A.-M.; Filinchuk, Y.; Tarascon, J.-M.; Férey, G. *Inorg. Chem.* **2010**, *49*, 7135−7143. (d) Nguyen, T. L. A.; Devic, T.; Mialane, P.; Rivière, E.; Sonnauer, A.; Stock, N.; Demir-Cakan, R.; Morcrette, M.; Livage, C.; Marrot, J.; Tarascon, J.-M.; Férey, G. *Inorg. Chem.* **2010**, *49*, 10710−10717.
(13) Feng, Y.; Zhang, Q.; Tan, W.; Zhang, D.; Tu, Y.; Ågren, H.; Tian, H. *Chem. Phys. Lett.* **2008**, *455*, 256−260.
(14) (a) Lee, J. Y.; Painter, P. C.; Coleman, M. M. *Macromolecules* **1988**, *21*, 954−960. (b) Kato, T.; Fréchet, J. M. J. *Macromolecules* **1989**, *22*, 3818−3819. (c) Bazuin, C. G.; Brandys, F. A. *Chem. Mater.* **1992**, *4*, 970−972. (d) St. Pourcain, C. B.; Griffin, A. C. *Macromolecules* **1995**, *28*, 4116−4121. (e) Luo, X. F.; Goh, S. H.; Lee, S. Y.; Tan, K. L. *Macromolecules* **1998**, *31*, 3251−3254. (f) Cooke, G.; Rotello, V. M. *Chem. Soc. Rev.* **2002**, *31*, 275−286. (g) Xu, J.; Toh, C. L.; Liu, X.; Wang, S.; He, C.; Lu, X. *Macromolecules* **2005**, *38*, 1684−1690. (h) Li, R.; Yang, X.; Li, G.; Li, S.; Huang, W. *Langmuir* **2006**, *22*, 8127−8133.
(15) (a) Wang, Z.; Zhang, D.; Zhu, D. *J. Org. Chem.* **2005**, *70*, 5729−5732. (b) Tan, W.; Wang, Z.; Zhang, D.; Zhu, D. *Sensors* **2006**, *6*, 954−961.
(16) Devic, T.; Avarvari, N.; Batail, P. *Chem.—Eur. J.* **2004**, *10*, 3697−3707.
(17) (a) McCullough, R. D.; Petruska, M. A.; Belot, J. A. *Tetrahedron* **1999**, *55*, 9979−9998. (b) Garin, J.; Orduna, J.; Uriel, S.; Moore, A. J.; Bryce, M. R.; Wegener, S.; Yufit, D. S.; Howard, J. A. K. *Synthesis* **1994**, 489−493.
(18) (a) Frisch, M. J.; Trucks, G. W.; Schlegel, H. B.; Scuseria, G. E.; Robb, M. A.; Cheeseman, J. R.; Montgomery, J. A., Jr.; Vreven, T.; Kudin, K. N.; Burant, J. C.; Millam, J. M.; Iyengar, S. S.; Tomasi, J.; Barone, V.; Mennucci, B.; Cossi, M.; Scalmani, G.; Rega, N.; Petersson, G. A.; Nakatsuji, H.; Hada, M.; Ehara, M.; Toyota, K.; Fukuda, R.; Hasegawa, J.; Ishida, M.; Nakajima, T.; Honda, Y.; Kitao, O.; Nakai, H.; Klene, M.; Li, X.; Knox, J. E.; Hratchian, H. P.; Cross, J. B.; Bakken, V.; Adamo, C.; Jaramillo, J.; Gomperts, R.; Stratmann, R. E.; Yazyev, O.; Austin, A. J.; Cammi, R.; Pomelli, C.; Ochterski, J. W.; Ayala, P. Y.; Morokuma, K.; Voth, G. A.; Salvador, P.; Dannenberg, J. J.; Zakrzewski, V. G.; Dapprich, S.; Daniels, A. D.; Strain, M. C.; Farkas, O.; Malick, D. K.; Rabuck, A. D.; Raghavachari, K.; Foresman, J. B.; Ortiz, J. V.; Cui, Q.; Baboul, A. G.; Clifford, S.; Cioslowski, J.; Stefanov, B. B.; Liu, G.; Liashenko, A.; Piskorz, P.; Komaromi, I.; Martin, R. L.; Fox, D. J.; Keith, T.; Al-Laham, M. A.; Peng, C. Y.; Nanayakkara, A.; Challacombe, M.; Gill, P. M. W.; Johnson, B.; Chen, W.; Wong, M. W.; Gonzalez, C.; Pople, J. A. *Gaussian 03*, revision B.01; Gaussian, Inc.: Wallingford, CT, 2003. (b) Becke, A. D. *J. Chem. Phys.* **1993**, *98*, 5648−5652 and references therein.
(19) (a) Becke, A. D. *Phys. Rev. A* **1988**, *38*, 3098−3100. (b) Lee, C.; Yang, W.; Parr, R. G. *Phys. Rev. B* **1988**, *37*, 785−789.
(20) *CrystalClear Software User's Guide*; Rigaku Molecular Structure Corporation: Orem, UT, 2000. Pflugrath, J. W. *Acta Crystallogr., Sect. D: Biol. Crystallogr.* **1999**, *55*, 1718−1725.
(21) Sheldrick, G. M. *SHELXS-97*, Program for Structure Solution; Universität of Göttingen: Göttingen, Germany, 1999.
(22) Sheldrick, G. M. *SHELXL-97*, Program for Structure Refinement; Universität of Göttingen: Göttingen, Germany, 1997.
(23) Koch, W.; Holthausen, M. C. *A Chemist's Guide to Density Functional Theory*; Wiley-VCH: Weinheim, Germany, 2000.
(24) Andreu, R.; Malfant, I.; Lacroix, P. G.; Cassoux, P. *Eur. J. Org. Chem.* **2000**, 737−741.
(25) (a) Le Derf, F.; Mazari, M.; Mercier, N.; Levillain, E.; Trippé, G.; Riou, A.; Richomme, P.; Becher, J.; Garín, J.; Orduna, J.; Gallego-Planas, N.; Gorgues, A.; Sallé, M. *Chem.—Eur. J.* **2001**, *7*, 447−455. (b) Le Derf, F.; Levillain, E.; Trippé, G.; Gorgues, A.; Sallé, M.; Sebastian, R. M.; Caminade, A. M.; Majoral, J. P. *Angew. Chem., Int. Ed.* **2001**, *40*, 224−227.
(26) Spek, A. L. *Platon-270705*, A Multipurpose Crystallographic Tool; Utrecht University: Utrecht, The Netherlands, 1980−2005.